Atmos. Meas. Tech., 16, 3123–3139, 2023
https://doi.org/10.5194/amt-16-3123-2023

Atmospheric Measurement Techniques
Open Access
EGU

Stratospheric-trace-gas-profile retrievals from balloon-borne limb imaging of mid-infrared emission spectra

Ethan Runge[1], **Jeff Langille**[2], **Daniel Zawada**[1], **Adam Bourassa**[1], **and Doug Degenstein**[1]

[1]Institute of Space and Atmospheric Studies, University of Saskatchewan, Saskatoon SK, Canada
[2]Physics, University of New Brunswick, Fredericton NB, Canada

Correspondence: Ethan Runge (ethan.runge@usask.ca)

Received: 20 January 2023 – Discussion started: 15 February 2023
Revised: 6 May 2023 – Accepted: 26 May 2023 – Published: 26 June 2023

Abstract. The Limb Imaging Fourier Transform Spectrometer Experiment (LIFE) instrument is a balloon-borne prototype of a satellite instrument designed to take vertical images of atmospheric limb emission spectra in the 700–1400 cm^{-1} wavenumber range from the upper-troposphere–lower-stratosphere (UTLS) altitude region of the atmosphere. The prototype builds on the success of past and existing instruments while reducing the complexity of the imaging design. This paper details the results of a demonstration flight on a stabilized stratospheric balloon gondola from Timmins, Canada, in August 2019. Retrievals of vertical trace gas profiles for the important greenhouse gases H_2O, O_3, CH_4, and N_2O, as well as HNO_3, are performed using an optimal estimation approach and the SASKTRAN radiative transfer model. The retrieved profiles are compared to approximately coincident observations made by the Atmospheric Chemistry Experiment Fourier Transform Spectrometer (ACE-FTS) solar occultation and Microwave Limb Sounder (MLS) instruments. An evaluation of the LIFE measurements is performed, and areas of improvement are identified. This work increases the overall technical readiness of the approach for future balloon, aircraft, and space applications.

1 Introduction

The Limb Imaging Fourier Transform Spectrometer Experiment (LIFE) is an imaging Fourier transform spectrometer (IFTS) developed by the University of Saskatchewan in collaboration with ABB Canada and with funding from the Canadian Space Agency. The eventual goal is to use vertical imaging from low earth orbit to obtain high-spatial-resolution atmospheric composition measurements in the upper-troposphere–lower-stratosphere (UTLS) region of the atmosphere (Runge et al., 2021). The current prototype uses a linear array detector and imaging optics designed to cover the limb altitudes from typical float altitude of a stratospheric balloon platform. The prototype is unique in design as it makes use of a modified commercially available interferometer, forgoes the use of fore-optics, and has only one cooled element in the form of a cold-stop assembly to mitigate the impact of instrument self-emission rather than using fully cooled optics. The first technology demonstration flight of the instrument was performed from a stratospheric balloon launched and operated by the Centre National d'Etudes Spatiales (CNES) from Timmins, Canada, in August of 2019. The development, characterization, and calibration of the instrument are detailed in-depth in an earlier publication (Runge et al., 2021). The current work details the approach to retrievals of trace gas profiles, and the results are characterized in terms of precision and resolution.

The prototype draws on several decades worth of community research and advancement in the field of FTS instruments as a method of remote sensing for atmospheric trace gases. The primary influence on the LIFE instrument is the Gimballed Limb Observer for Radiance Imaging of the Atmosphere (GLORIA). GLORIA is an IFTS designed for aircraft and balloon platforms and has very similar goals and design elements to LIFE (Riese et al., 2014; Friedl-Vallon et al., 2014). Prior to the development of LIFE, GLORIA had been validated using measurements from several campaigns and produced rich datasets indicating the robustness of the concept (Johansson et al., 2018; Sha, 2013; Kleinert et al., 2014; Olschewski et al., 2013; Monte et al., 2014;

Kaufmann et al., 2015; Piesch et al., 2015; Ungermann et al., 2015). The goal of the LIFE prototype was to build on these successes and create an instrument of similar capabilities with less complexity. The spectra obtained from the LIFE demonstration flight indicate that design specification goals were met, though residual issues with radiometric calibration remain (Runge et al., 2021).

Critical heritage for these instruments comes from the Michelson Interferometer for Passive Atmospheric Sounding (MIPAS), the forebear of GLORIA. While MIPAS is not an imaging instrument (i.e. it uses a single-element detector instead of an array), many aspects of the design are applicable to both GLORIA and LIFE (Fischer et al., 2008; Friedl-Vallon et al., 2004; Fischer and Oelhaf, 1996). The approach to trace gas retrievals from the MIPAS reduced-resolution mode provides valuable insight into the choice of spectral windows used for the LIFE retrievals (Fischer and Oelhaf, 1996; von Clarmann et al., 2009).

In this study we also use measurements from the Atmospheric Chemistry Experiment Fourier Transform Spectrometer (ACE-FTS) and Microwave Limb Sounder (MLS) instruments. ACE-FTS has been operational on board SCISAT for nearly 2 decades and provides limb measurements at dusk and dawn via solar occultation (Bernath et al., 2005). Measurements made by ACE have been validated against other satellite instruments and ground-based and aircraft-based sources and are generally accepted as accurate (Walker et al., 2005; Waymark et al., 2014; Walker et al., 2018, 2021). Each of the target species we retrieve here with LIFE have been validated for ACE-FTS: H_2O (Weaver et al., 2019; Davis et al., 2021; Sheese et al., 2017), O_3 (Bognar et al., 2019; Sheese et al., 2022, 2017), N_2O (Sheese et al., 2017; Plieninger et al., 2016), and CH_4 (Plieninger et al., 2016). Additional species like HNO_3 have also been validated (Sheese et al., 2017). Due to the high coverage and availability of data at the time of the Timmins flight, trace gas profiles determined from ACE measurements provide a good benchmark by which to judge the validity of the profiles returned by the LIFE data analysis. Additional coverage and comparison are provided by measurements taken from the MLS, which makes use of heterodyne radiometers measuring in the thermal regime (Waters et al., 2006). Similar to LIFE, GLORIA, and MIPAS, thermal-emission measurements allow the MLS to take measurements during both day and night without the need for external sources, greatly increasing the potential coverage (Waters et al., 2006). The MLS measurements have been validated for all target species except CH_4, which it does not measure: H_2O (Lambert et al., 2007; Vömel et al., 2007; Barnes et al., 2008; Hurst et al., 2014), O_3 (Jiang et al., 2007; Froidevaux et al., 2008), N_2O (Lambert et al., 2007), and HNO_3 (Santee et al., 2007). A comparison to several ACE and MLS profiles taken close to the day of the LIFE flight is included as a verification that the LIFE prototype meets the scientific goals in addition to the design specifications indicated in the prior publication (Runge et al., 2021).

In this paper, the retrieval algorithm used to determine the trace gas profiles is first described in a general sense. A more detailed accounting of how the general algorithm is modified for the particular aspects of the LIFE instrument follows, along with a description of the trace-gas-profile determination for each of the species of interest. Following the individual description of the retrieved quantities, a direct comparison of generally accepted profiles obtained from ACE measurements is done to demonstrate the quality of the LIFE profiles, verifying that the prototype concept achieves the scientific goals. These results show the validity of utilizing commercially available off-the-shelf components and simpler optics for reduced cost and un-cooled optics for reduced complexity, marking attractive options for future space-based instruments.

2 LIFE instrument

The LIFE instrument is made with several custom-made anodized aluminum cases containing the optics, control electronics, and blackbodies. The optical path starts with a pointing system that can be aimed to view the atmospheric limb through one port or at either of the onboard blackbodies through other ports. The interferometer at the core of the instrument is a modified version of the commercially available MB3000 interferometer manufactured by ABB Canada. The aft-optics are custom-made lenses and focus the system on a 16-element mercury cadmium telluride (MCT) detector, with a cold-stop cooled by an onboard sterling cooler to reduce the self-emission signal.

The full field of view (FOV) of the instrument is 6.01°, with each pixel covering 0.32°. At the in-flight float altitude of 40 km, this FOV resolution results in a tangent altitude spacing of about 4 or 5 km between pixels. An interferogram is generated for each pixel every 2.26 s as the interferometer moves through the full −1.4–1.4 cm optical path difference (OPD) range. The OPD leads to a spectral sampling of 0.357 cm^{-1} over the spectral range, 700 to 1400 cm^{-1}, for which LIFE measurements are taken.

Retrieval performance requires a noise-equivalent spectral radiance (NESR) of 15 $nW\,cm^{-2}\,sr^{-1}\,(cm^{-1})^{-1}$ (Runge et al., 2021). Individual scans have a higher noise than this, and so time averaging is performed. For the measurements presented in this paper, 20 scans are averaged together, reducing the temporal cadence of the instrument to 45 s. The full characterization and description of the instrument is detailed in the LIFE instrument paper by Runge et al. (2021).

3 Retrieval

3.1 Overview

The retrieval method applied to the LIFE data follows the atmospheric inverse-problem solution described in

Rodgers (2000) and uses similar notation. The goal of this approach is to take a given set of measurement information, the measurement vector $\boldsymbol{y}$ with length m that contains the instrument spectra obtained from the instrument, and determine a set of atmospheric state parameters, the state vector containing the atmospheric concentrations to be retrieved and other instrument parameters, $\boldsymbol{x}$ of length n, that determine the state of the atmosphere. The state vector is input to a forward model, F, that represents the physics of the atmosphere and the instrument to obtain a set of expected radiances. The inverse method is then concerned with iteratively changing the state vector until the forward model output matches the measurement vector. The iterative approach determines how the state vector should be changed via minimization of the cost function

$$\chi^2 = (\boldsymbol{y} - F(\boldsymbol{x}))^{\mathrm{T}}\mathbf{S}_{\epsilon}^{-1}(\boldsymbol{y} - F(\boldsymbol{x})) + (\boldsymbol{x} - \boldsymbol{x}_{\mathrm{a}})^{\mathrm{T}}\boldsymbol{\Gamma}^{\mathrm{T}}\boldsymbol{\Gamma}(\boldsymbol{x} - \boldsymbol{x}_{\mathrm{a}}), \quad (1)$$

where $\mathbf{S}_{\epsilon}$ is the error covariance matrix associated with the measurement vector, $\boldsymbol{x}_{\mathrm{a}}$ is the a priori state vector, and $\boldsymbol{\Gamma}$ is a regularization matrix that determines the influence of the a priori state on the minimization. The elements of $\mathbf{S}_{\epsilon}$ are calculated from the measurement noise after spectral calibration. Using the Gauss–Newton minimization method leads to the iterative step formula

$$\boldsymbol{x}_{i+1} = \boldsymbol{x}_i + \left(\mathbf{K}_i^{\mathrm{T}}\mathbf{S}_{\epsilon}^{-1}\mathbf{K}_i + \boldsymbol{\Gamma}^{\mathrm{T}}\boldsymbol{\Gamma} + \gamma_i \mathrm{diag}\left(\mathbf{K}^{\mathrm{T}}\mathbf{S}_{\epsilon}{}^{-1}\mathbf{K}\right)\right)^{-1} \times \left[\mathbf{K}_i^{\mathrm{T}}\mathbf{S}_{\epsilon}^{-1}(\boldsymbol{y} - F(\boldsymbol{x}_i)) - \boldsymbol{\Gamma}^{\mathrm{T}}\boldsymbol{\Gamma}(\boldsymbol{x}_i - \boldsymbol{x}_{\mathrm{a}})\right], \quad (2)$$

with $\mathbf{K}$ representing the Jacobian matrix of the forward model; i the step number; and γ a Levenberg–Marquardt damping factor, which aids in the convergence of the Gauss–Newton method in non-linear cases (Fletcher, 1971).

Also of importance in the discussion of the retrieval is the averaging kernel, as it gives an indication as to the effective vertical resolution of the retrieved profile. The averaging kernel is defined as

$$\mathbf{A} = \left(\mathbf{K}^{\mathrm{T}}\mathbf{S}_{\epsilon}^{-1}\mathbf{K} + \mathbf{S}_{\mathrm{a}}^{-1}\right)\mathbf{K}^{\mathrm{T}}\mathbf{S}_{\epsilon}^{-1}\mathbf{K}, \quad (3)$$

with the newly defined $\mathbf{S}_{\mathrm{a}}^{-1} = \boldsymbol{\Gamma}^{\mathrm{T}}\boldsymbol{\Gamma}$. The averaging kernel shows how each retrieval grid point depends on its neighbours. As such, the full width at half max (FWHM) for a given row of the averaging kernel is an indication of the vertical resolution of the retrieval. This can be modified by regularization factors, discussed further in Sect. 3.6.

Due to unique systematic artefacts within the LIFE measurement vector, the retrieval approach for atmospheric trace species needs to occur in a cycle of two or three retrievals, each solving for a different set of state vectors. The cycle required for each quantity of interest is discussed in the respective subsection of Sect. 4. The retrieval process applied at any of the stages is depicted by the flowchart in Fig. 1.

Each of the quantities sought uses the calibrated spectra and the results of the previously obtained quantity in the retrieval process. The flowchart depicted in Fig. 2 shows the general retrieval order. For each time-averaged set of measurements, the pointing is found first with the proper microwindow, which is followed by H_2O. The retrieved profile is input into the climatology, replacing the standard H_2O profile for the next species retrieval, which is O_3. The process continues by replacing atmospheric profiles in the climatology with the retrieved profile; HNO_3 comes after O_3 and then CH_4 and N_2O. Also note in this schema that no retrieval of temperature is done due to uncertainty in radiometric calibration accuracy. The Modern-Era Retrospective analysis for Research and Applications (MERRA) temperature profile is used instead, which leads to some errors, as discussed in Sect. 4.2.1.

3.2 Forward model

The forward model consists of a radiative transfer model and an instrument model. The radiative transfer model portion makes use of the SASKTRAN radiative transfer framework. The original framework was developed at the University of Saskatchewan to provide efficient estimation of limb scatter measurements as a function of wavelength and tangent altitude (Bourassa et al., 2008). The model uses a successive-order approach to calculate measurements along rays traced through a spherical atmosphere. Since the initial inception, updates have been made to the framework to allow for the accurate calculation of high-spatial-resolution measurements in a non-spherically symmetric atmosphere, increasing the accuracy of the estimates (Zawada et al., 2015). This framework is referred to as SASKTRAN-HR. Further improvements to SASKTRAN-HR have been made that allow the analytic calculation of weighting functions, increasing the speed of calculations by many orders of magnitude (Zawada et al., 2017).

The most recent improvement to the SASKTRAN radiative transfer engine critical to the LIFE analysis is the development of a thermal radiative transfer model, known as SASKTRAN-TIR. The implementation of the thermal radiative transfer engine is detailed in Warnock (2020) and Jensen (2015). The framework breaks the atmosphere into a series of cells along the instrument lines of sight (LOSs). Starting at the furthest point from the defined observer, the cell contributions are determined and passed as an input to the next cell in the series. The total contribution of all cells, attenuated through each LOS, is determined at the observer location. Spectral line intensities are calculated from the HIgh-resolution TRANsmission molecular absorption (HITRAN) database, utilizing the HITRAN2016 (Gordon et al., 2017) database for this implementation. The simulated environment implemented to generate high-resolution output is made with standard Fast Atmospheric Signature CODE (FASCODE) atmospheric constituents for

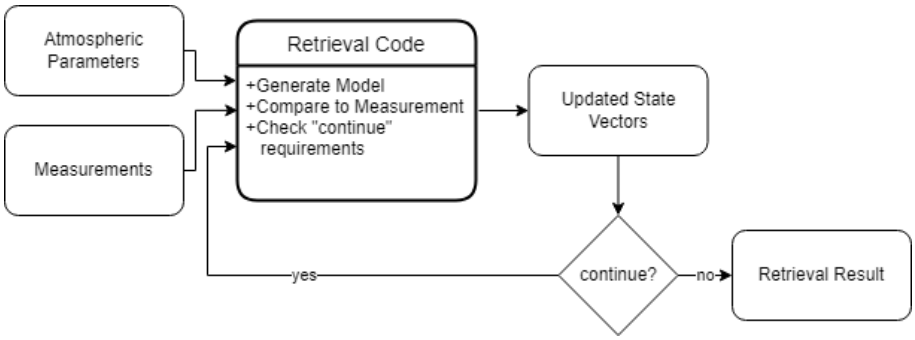

Figure 1. The general process used by the retrieval code. Inputs are given to the code as initial parameters, a comparison is made, and the parameters that the code has access to change (the state vectors) are updated. A set of requirements are provided on whether more iterations are needed. If more are needed, the updated state vector is used as the new input. If the completion criteria are met, the updated state vector output is the result.

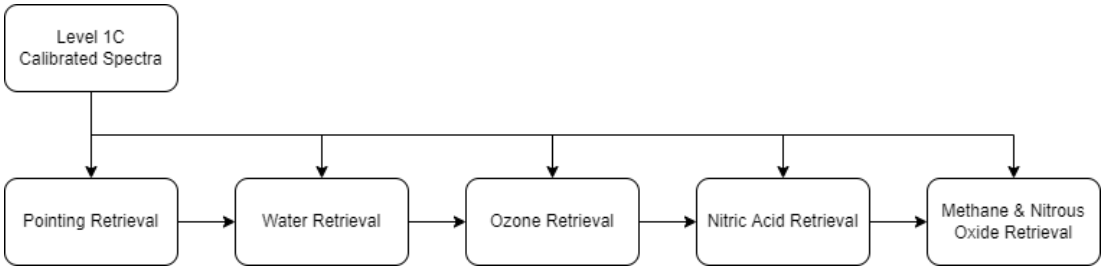

Figure 2. Broad flowchart for the determination of trace gas profiles applied to each scan of the LIFE data. Each of the stages is further divided into a retrieval process.

most species (Anderson et al., 1986; Clough et al., 1987), SASKTRAN's built-in Labow ozone profile, and MERRA temperature and pressure profiles (Global Modeling and Assimilation Office, 2015). Voigt broadening profiles of the HITRAN spectral lines are calculated based on the provided MERRA temperature and pressure profiles.

The instrument model portion of the forward model takes the radiative transfer results and performs a convolution with the instrument line shape (ILS) based on instrument parameters. The LIFE instrument has 16 pixels with well-known and consistent FOV values. The model is set up with an observer at a given height and LOS vectors. This information is also given to SASKTRAN such that the radiative transfer model generates measurements over the same LOS range as the LIFE measurements but at a much higher LOS density. Each pixel has an initial pointing vector, a calculated pitch correction, and a known non-zero FOV which define its light collection properties within the simulation. These three attributes work in conjunction with one another to create integration weights which are then applied to the high-density LOS model. This effectively performs a weighted average of the modelled signal for a given LOS and FOV in a manner that is representative of the physical operation of the LIFE instrument. The result is a high-resolution spectrum for each of the LOSs, an example of which is given in Fig. 6b as a representative radiance incident onto the instrument. These high-resolution radiance spectra are used as input to the front end of the high-fidelity instrument model that simulates real instrument effects such as the broadening due to instrument line shape.

3.3 Spectral windows

The retrieval spectral windows used in the LIFE retrievals are broadly based on microwindows used by von Clarmann et al. (2009) for MIPAS, since they are chosen for sensitivity in this spectral/altitude range, and optimal exclusion of non-local-thermodynamic-equilibrium (non-LTE) emissions. However, because of the relatively lower spectral resolution of the LIFE measurements we have often chosen broader ranges in this application. While admittedly not an optimal set in the sense of von Clarmann et al. (2009), these make a reasonable choice for demonstration of proof-of-concept retrievals. The windows used are given in Fig. 3. The left panel of the figure is a table indicating the species name and the wavenumber range with a coloured background associated with that species. The right panel shows the full extent of the LIFE wavenumber range for each of the measurement LOS paths. The coloured areas show the location of each of the corresponding species' spectral windows in the larger spectral range.

Species	Microwindow Range (cm^{-1})
H_2O	1353 - 1376
O_3	760 - 790
	1020 - 1040
HNO_3	875 - 885
CH_4 and N_2O	1227 - 1236
	1272 - 1304

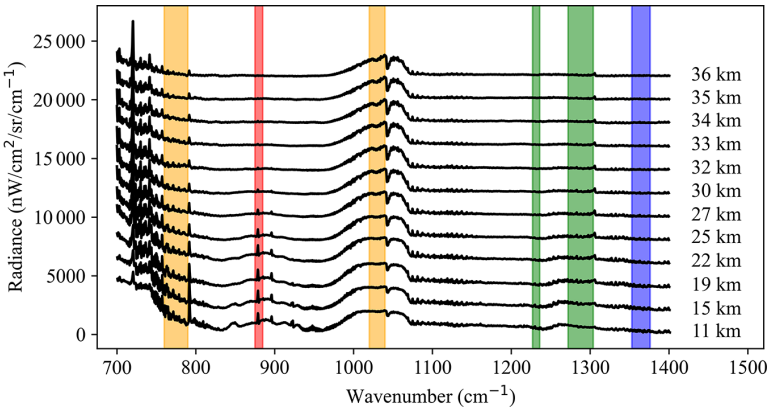

Figure 3. Spectral windows used in the LIFE retrievals. Each coloured spectral span corresponds to the species with corresponding background colour. Only 12 tangent heights are shown here for clarity; the bottom-most pixel LOS views the ground and is thus omitted, and the top three have tangent altitudes in the 36 km range and are omitted to prevent crowding.

3.4 State vector

The state vector consists of state elements, individual parameters that the retrieval is allowed to modify in the retrieval process, which are used as input to the forward model. This typically includes the target species concentrations and instrumental factors. In the case of target-trace-gas-species profiles, the state vector contains concentrations in terms of parts per million by volume (ppmv) at discrete grid points with a spacing of 1000 m in the range covered by LIFE, approximately 11 to 40 km. The choice of parts per million by volume is made in this particular case since the profiles are smoother than number density retrievals.

LIFE takes simultaneous measurements along each LOS instead of using a scanning technique. This means that every LOS measurement is taken by a different pixel, each requiring special corrections for systematic biases and artefacts remaining in the radiometrically calibrated data (Runge et al., 2021). Each pixel has a series of state elements that are used to correct issues that may still exist after the radiometric calibration. These come in the form of a radiometric offset to shift the baseline, a radiometric slope to correct for systematics appearing in select microwindows, and a shift in the spectra to accurately register wavenumber. These three correction parameters are unique for each of the microwindows used in the retrieval process. A final state element used for the LIFE measurements is a continuum profile that is used to correct for baseline shifts that cannot be corrected for with radiometric offsets or slopes.

3.5 Retrieval order

The first step in obtaining a complete set of retrieved profiles is the determination of the instrument pointing. Figure 4 depicts the process for pointing determination, where the pointing parameter is the only kept value, used in every subsequent species retrieval from the same time period. The core section "pointing retrieval" follows the process from Fig. 1.

Onboard telemetry and knowledge of the pointing mirror orientation allow a close determination of the instrument pointing, but even with care taken to choose a stable time period, the averaging in time required to meet noise constraints means that some error in the pointing is expected (Runge et al., 2021). In this case, an appropriate shift to the instrument pointing is determined for the time period from which the measurements are taken. CO_2 windows are chosen for the pointing retrieval due to the trace gas being nearly homogeneous in the atmosphere and having little altitude dependence (von Clarmann et al., 2009).

Trace gas retrievals then follow in the order of H_2O, O_3, HNO_3, and CH_4 joined with N_2O. A detailed breakdown of the water retrieval process for example is given in Fig. 5. Each of the "stage" blocks in this flowchart follows the process set out in Fig. 1.

The water retrieval's first stage takes as input a standard atmosphere, the LIFE measurements, three initial correction state vectors, and the previously determined pointing as a frozen parameter. These state vectors allow a wavenumber shift to align peaks and both a constant and linear radiometric correction to remove residual radiometric correction errors in the baseline. The correction state vector results are saved for use in the second stage, where a continuum correction is added as a variable. The initial states for Stage 2 are the results from Stage 1, with the spectral shift vector no longer being allowed to change. In Stage 3 the spectral shift and continua are frozen, the previous Stage 2 radiometric corrections are used as an initial guess that can be modified by the process, and the water profile is now allowed to change. At the end of this step, the water profile is determined. Similar processes to Fig. 5 are applied to O_3, HNO_3, and the co-retrieved CH_4 and N_2O, though H_2O is the most

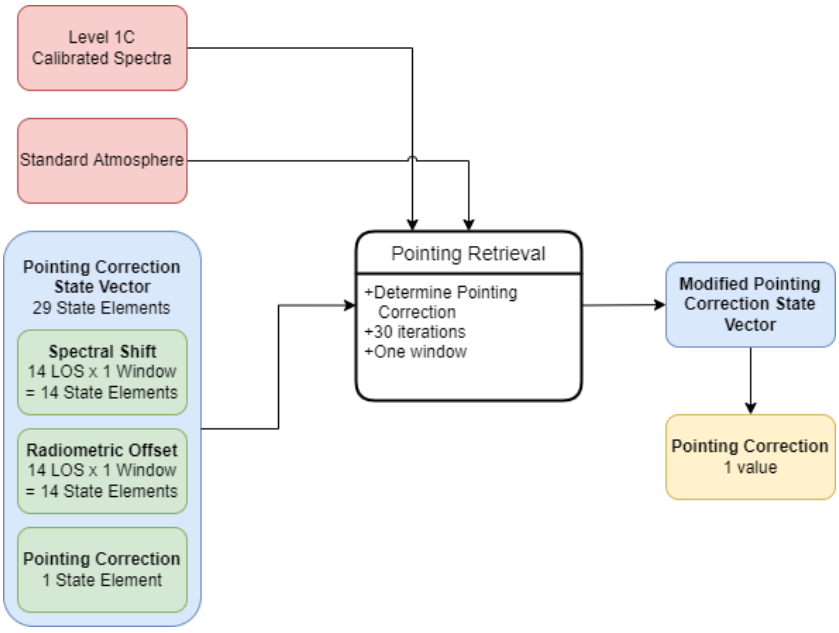

Figure 4. The pointing retrieval takes as input a standard atmosphere and state vectors allowing pointing, spectral shift, and radiometric offset to change and returns the pointing angle parameter associated with the best fit.

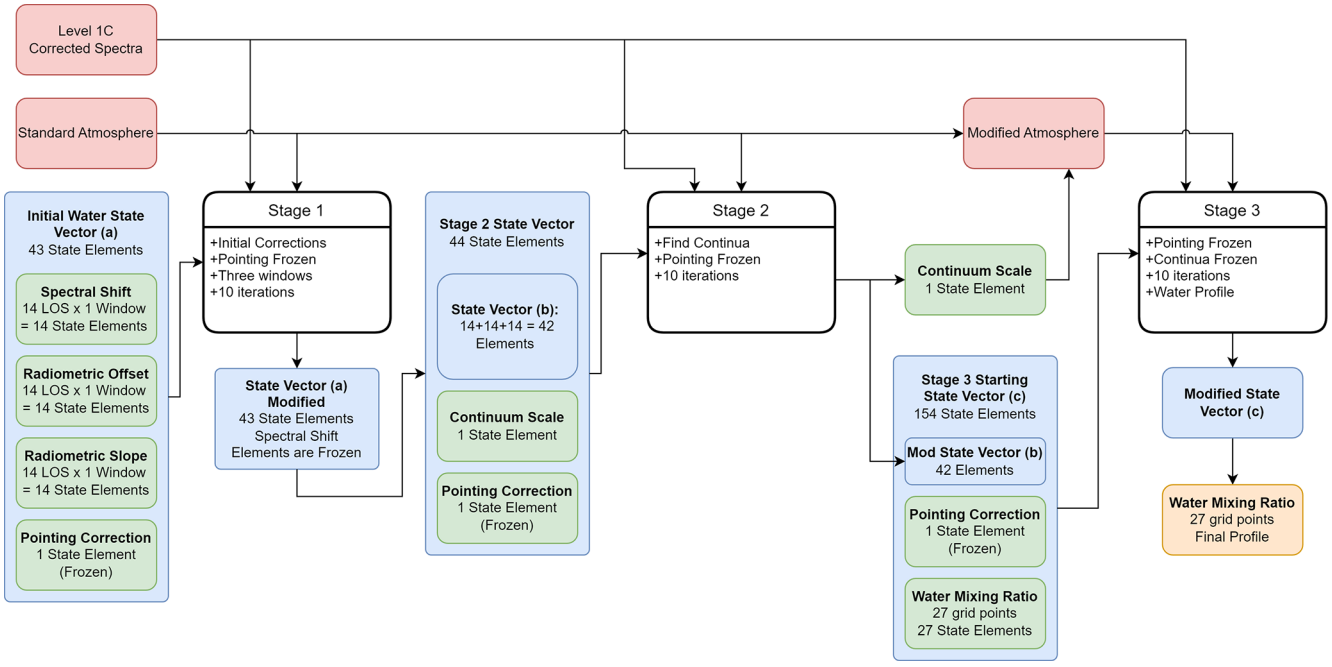

Figure 5. Breakdown of the H_2O profile retrieval step for LIFE instrument scans. Red boxes indicate parameters set by methods other than the state vectors, blue boxes represent state vector parameters, and green boxes are user-defined parameters. The orange box represents the final output of the retrieval process.

complicated. Section 4.2 describes more in-depth the state vectors and the necessity of each parameter.

In general, the trace gas profile determined in the previous retrieval is used as an input in subsequent retrievals, as shown in Fig. 2. Pointing is used as an input for H_2O, then pointing and the H_2O profile are used for O_3, etc. In this way, major contributors to the thermal signal are determined first to minimize their ability to skew results for those species with smaller contributions.

3.6 Regularization

The vertical profile grid utilized in the LIFE retrievals is finer than the measurement grid, leading to large oscillations in the trace-gas-profile solutions unless regularization is applied. A second-order Tikhonov regularization is applied to the averaging kernel to smooth the profile by inducing a dependence of each point of the retrieved concentration profile on the neighbouring points. This smoothing will also reduce the effective resolution of the retrieved profile to less than the initial retrieval grid. The effective resolution for each of the retrieved grid points is given by the FWHM of the averaging kernel associated with that grid point. For each of the retrieved species, a regularization factor determining the strength of the dependence on neighbouring points is chosen such that the FWHM is close to the measurement vertical resolution, about 5 km on average, when possible. Regularization above the measurement resolution begins to average information from different measurement vectors and results in information loss with respect to the profile structure. Section 4.2.4 details the averaging kernel and resulting vertical resolution for each of the species retrievals.

4 Retrieval implementation and results

4.1 Process and pointing

To retrieve trace gas profiles from the LIFE measurements, the processing chain must begin with a correction to the LOS pointing angles. The methodology and need for this correction are identified in von Clarmann et al. (2009), where CO_2 is used to correct for the pointing of the MIPAS instrument. For the LIFE prototype we follow this example, using CO_2 as well, covering most of the same range as was used in the MIPAS case, 745 to 765 cm^{-1}, as this is a window where the features are not heavily obscured by other atmospheric species (von Clarmann et al., 2009). The correction to pointing information retrieved from the flight gondola is deemed necessary due to uncertainties in the gondola stability over the time of measurements that are averaged together and the consistency of the pointing apparatus employed by the instrument. Using a known quantity such as CO_2, which is determined from observations made at the Mauna Loa National Oceanic and Atmospheric Administration (NOAA) facility at the time of flight (408 parts per million, ppm), allows the retrieval to find the optimal pointing correction (https://www.esrl.noaa.gov/gmd/ccgg/trends/monthly.html, last access: 14 January 2023). A representative measurement made by one of the pixels after the 45 s time averaging is applied and is shown in Fig. 6a.

As per the discussion of Sect. 3.2, the initial pointing vectors are generated from flight data retrieved from the gondola. In Fig. 6b the forward model's intermediate steps of determination of the high-resolution output of the radiative transfer model along an LOS and the ILS for the corresponding pixel it is to be convolved with are depicted. The blue line in Fig. 6c shows the first spectrum of the retrieval process based on initial parameters. The orange line in this figure shows the result after one iteration that is allowed to change correction parameters, which can be seen to be much closer to the measurement than the prior attempt.

All LOS vectors are adjusted using the same correction factor, and the state vector is updated, as depicted in the flowchart of Fig. 4. The next iteration starts, using the updated state vector to generate new results. This process continues until pre-defined criteria are met, in this case 30 iterations.

Figure 6d shows the pitch, or tangent altitude, correction factor as a function of the iterations, where it is seen to converge after approximately 20 iterations, after which further changes are minuscule. The value that the retrieval converges to is $-3.269 \pm 0.014 \times 10^{-3}$ rad, which is an upward tilt of just over 0.2°.

4.2 Trace atmospheric gases

Trace gas retrievals follow much the same process as the preceding pointing correction retrieval. The state vector for each consists of the volume mixing ratio in parts per million volume on the defined atmospheric grid of the SASKTRAN model, which is in 1 km steps in this case, as well as the parameters for correction of the per-pixel radiometric calibration, per-pixel spectral shift, and the previously retrieved pointing correction. Note that the pointing correction is required in the state vector to update the states properly but is no longer allowed to vary.

Due to the large number of unknowns in the state vector, retrieval of all parameters at once often leads to poor convergence and non-physical results. The solution is to break each species retrieval into two or three stages, an example of which is shown in Fig. 5 for the H_2O retrieval specifically. The following description uses the specific example of the water retrieval to discuss the process, though each of the species has slightly different requirements.

In the first stage, the pointing previously determined is held constant while allowing the spectral shift and radiometric correction parameters to change. This can be seen as the "State Vector (a)" in Fig. 5. Taking the calibrated spectra and an unmodified atmosphere along with the state vector, the Stage 1 retrieval seeks to find the optimal fit for broad baseline features and spectral peak locations. This result is shown as "State Vector (a) Modified" in Fig. 5. This provides a much closer starting point for the following stages, allowing the minimizer to focus on more relevant parameters. For most species, this modified state vector has the spectral shift frozen and is then used as an input for the next stage. For water however, each window needs to be treated separately for computation, leading to Stage 2 running three times.

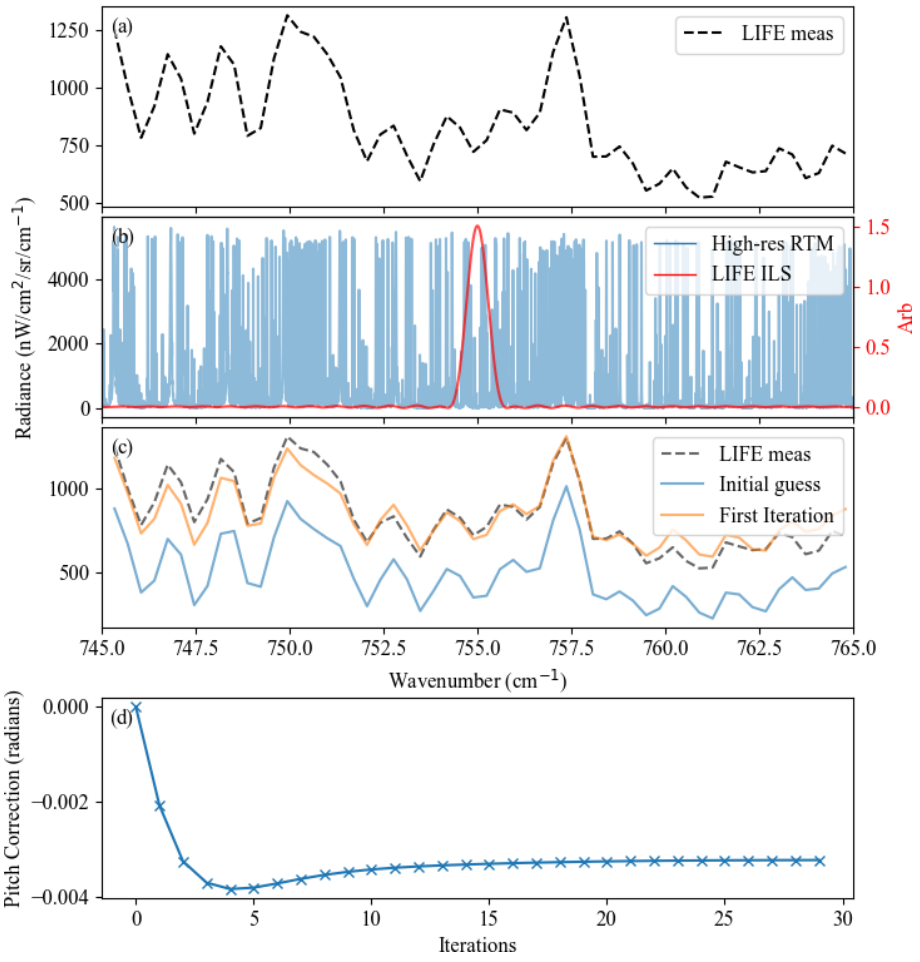

Figure 6. The stages of the LIFE pointing retrieval at specific points in the process. Panel **(a)** depicts the initial measurement for pixel 6, a pixel with LOS crossing near 27 km tangent altitude prior to correction. Panel **(b)** shows the high-resolution result of the integration weights from the high-resolution LOS grid for the pixel, overlaid with the instrument ILS. Panel **(c)** shows the LIFE measurements with the initial guess before any corrections are applied and the state of the modelled measurements after a single iteration. Panel **(d)** shows how the pointing correction changes as the retrieval goes through iterations. Note that a negative pointing correction corresponds to an upward tilt.

The second stage, for the species which require it, is an additional correction for an almost wavenumber-independent background signal in the form of a continuum. In real measurements, the baseline is increased by spectral contributions from outside the bounds of the microwindow but leaves spectral peaks within the microwindow unaffected. In simulated data, the wavelengths used are only for a small spectral range outside of the microwindow, and thus these effects may not be accurately represented by the model. The continuum profile aims to address this by providing the same functionality to the model with the introduction of a constant emission source over the spectral range. This continuum profile is an exponential curve as a function of altitude, multiplied by a variable scale factor that can be modified by the retrieval. In the case of the workflow of Fig. 5, continua are added as state vector parameters in each of the Stage 2 input state vectors for all species excepting HNO_3, for which the correction is not necessary. Stage 2 allows adjustment of the radiometric correction parameters in response to changes in the applied continua, though the spectral shift is frozen to further changes, as the wavenumber scale has been accurately registered after Stage 1. The general process of Fig. 1 is followed in each of the Stage 2 blocks.

The continuum profiles for each of the microwindows are added to the simulated atmosphere for Stage 3, excepting the HNO_3 case, as previously mentioned. For computation speed, rather than having the continua scale factors frozen as part of the Stage 3 state vector, the continua profiles are generated with the Stage 2 scale factors found and then added to the modified atmosphere. Stage 3 follows the general process of Fig. 1 using the first-stage spectral correction as a frozen parameter and the Stage 2 radiometric corrections as the initial status of the state vector. The trace gas parts per million volume mixing ratio at each of the defined atmospheric grid

points is finally added to the state vector as a parameter in this stage. The three-stage method results in a more reasonable fit, as the amount of correction required is reduced, and the adjustments to all parameters can be optimized together.

4.2.1 Error sources

In each of the retrievals, the primary sources of error are determined. The noise error in each trace gas profile is calculated as part of the retrieval process. The other major identified sources are the pointing, uncertainty in the ILS, and uncertainty in the MERRA temperature profile. Figure 7 shows the process for determining the error values that are given to all species.

In the case of pointing, the retrieval outlined in Fig. 4 prescribes both a correction factor and an expected error in that value. As per Fig. 2, a small error in pointing affects all species retrievals. For each of the species, Stage 3 is re-run with the pointing modified by the expected pointing error, which only slightly modifies the profile. The difference between this new profile and the originally retrieved profile is then considered to be the error caused by the pointing correction uncertainty, which is depicted in the central panels of Figs. 8 and 9 in yellow.

The ILS error works on the same principle as the pointing in that a small change is made in the third stage of the retrieval and re-run to obtain a profile that includes the error. A series of measurements taken in-lab with a thermal laser indicate that the uncertainty in the FWHM of the ILS in the unapodized case is about 0.01 cm^{-1}. The sinc function used as the ILS in the instrument model is broadened by this amount during the new Stage 3 profile determination. The difference between this and the original determination is considered to be the error in profile due to uncertainty in the ILS, given in green in the central column panels of Figs. 8 and 9.

The MERRA temperature profile derived from MLS measurements used in this analysis is considered to have an accuracy of 1 K or better in the altitude ranges considered by LIFE (Schwartz et al., 2008). Assuming the worst-case scenario, the temperature profile is modified, and all stages are re-run. The error in the profile is considered to be the difference between the result of the modified profile and the original. This error is given in red in the central panels of Fig. 8 and 9 and can be seen to dominate the profile error.

4.2.2 Single-species retrieval results

O_3 and HNO_3 retrievals are similar to H_2O in that the spectral peaks sought within the microwindows are relatively distinct with little overlap with other species, allowing a retrieval of the species individually using the three-stage methodology shown in Fig. 5. After the pointing is optimized, water becomes the most important profile to determine, due to the broad spectral emission range. The windows used here once again are broadened versions of those used in von Clarmann et al. (2009), divided into the three major regions shown in the table in Fig. 3. The result for H_2O is shown in the top two panels of Fig. 8. The black lines show the profile at the initial guess stage and after each iteration of the retrieval code. The green profile is the finalized result at the end of the 10th iteration, with a shaded green area indicating the extent of the error from all sources. These errors are difficult to see on the scale of the profile and are shown explicitly on a smaller scale in the center panel. The major contributor to water uncertainty is temperature uncertainty, with noise as the second-largest source. The water profile converges quickly, changing minimally after the third iteration. The final water profile has a shape similar to the initially provided FASCODE profile but shows a higher amount of oscillation. The right-hand panel shows that the water retrieval over the course of time is relatively stable, with no major outliers but with the small-scale structure varying from scan to scan.

Water is followed by ozone as the next major contributor in the atmosphere, shown in the second-row panels of Fig. 8. Ozone makes use of the two microwindows indicated in the table in Fig. 3. As in the water case, in Fig. 8, the black lines show the result after each iteration, and the green lines show the final result with a shaded error zone. The error source breakdown shows that the uncertainty in the vertical profile due to noise, ILS, and pointing uncertainty is minimal compared to temperature uncertainty. For each of the time windows, the corresponding ozone profile replaces the standard for subsequent retrievals. The right-most panel for ozone in Fig. 8 shows that the variation in ozone profiles, particularly at higher altitudes, seems to vary and drift, with some scans indicating a profile with less small-scale structure and others having more.

The final species retrieved in the single-species format is HNO_3. While not originally one of the science goals of the LIFE mission, the measurements show a strong and distinct spectral signal in the HNO_3 microwindows defined in von Clarmann et al. (2009). The iterations show again that minimal changes are made beyond the third iteration, indicating a quick convergence to the solution, and the error breakdown shows that the major uncertainty comes primarily from temperature uncertainty, with measurement noise being the next major contributor. The variance seen through different retrievals from differing time periods shows that these retrievals are fairly stable over time as well.

4.2.3 Coupled-species retrieval results

Methane (CH_4) and nitrous oxide (N_2O) have significant overlap in their defined window and are best retrieved together as a joint retrieval. This methodology has been shown to work for an established source, so it is considered to be a valid approach for LIFE as well (von Clarmann et al., 2009). This joint retrieval is further complicated by a substantial systematic instrument artefact in one of the microwindows,

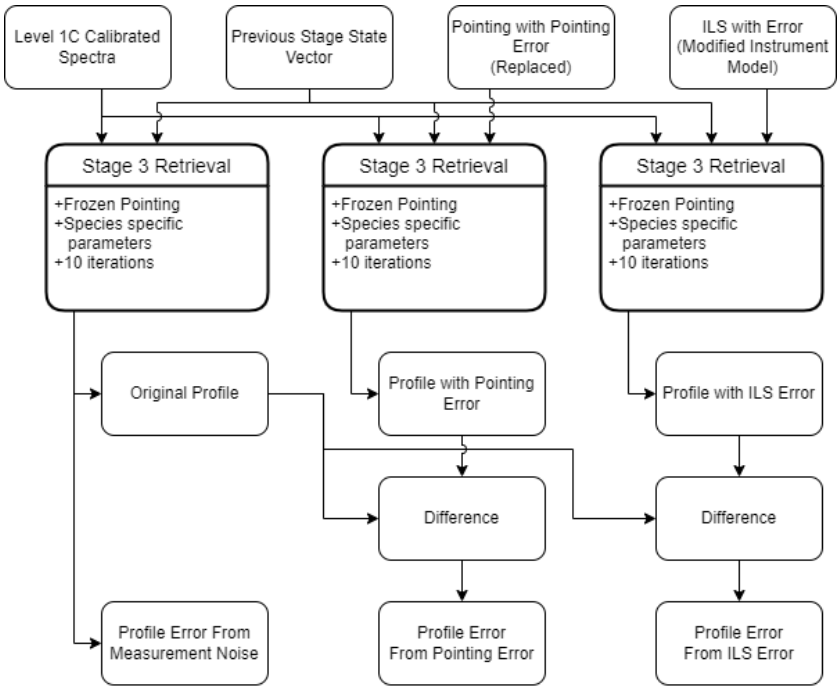

Figure 7. A flowchart depicting the process for determining the profile error resulting from each of the major identified error sources. This process is followed for each species. The Stage 3 block consists of the process depicted in Fig. 1.

requiring a radiometric slope correction parameter in addition to radiometric offset. Methane, in the top panel of Fig. 9, shows a structure similar to ozone, where it is higher than the initial profile at high altitudes and then lower around 28 km. Nitrous oxide shows the largest deviation from initial profile information out of any retrieved species, with the result indicating that the abundance is negligible at high altitudes before rising to a large peak at lower altitudes. These two profiles raise some interesting questions, particularly N_2O with the peculiar profile shape. Considering the nature of the spectral overlap of the species with the remaining systematic error, these retrievals warrant further investigation. The plausibility of these profiles is discussed more in Sect. 5. The center panels of Fig. 9 show that the temperature uncertainty is once again the dominant source of error in the profiles, though the systematic error is expected to have a large influence on these results with no clear method of determining the full extent. The right-hand panel shows that the stability of these results in time has a large amount of variability, especially below 25 km.

4.2.4 Averaging kernels and vertical resolution

The atmospheric grid on which the mixing ratio for each species is determined is finer than the measurement grid, leading to a need for regularization to deal with oscillations resulting from an under-defined problem. Regularization smooths the oscillations present in such solutions at the cost of increasing the vertical resolution. Each trace gas has a different factor applied to the second-order Tikhonov regularization matrix used for regularization in a way that balances oscillation reduction with maintaining a reasonable altitude resolution. In general, the resolution after smoothing should not be much greater than the altitude spacing of the measurements, meaning that for the LIFE prototype the aim is to ensure that the maximum vertical resolution remains close to 5 km when possible. The vertical resolution is determined by calculating the FWHM of the averaging kernel used in the retrieval. Figure 10 shows the averaging kernels for each of the species in the four left-hand panels. The rightmost panel of this figure shows the FWHM for each species as calculated from the averaging kernels.

The water and methane panels show much wider averaging kernels than the other species and consequently larger FWHM as a function of altitude. The reason for this is that the vertical profile retrievals of both species require more rigorous regularization. The FWHM of water peaks at just under 8 km, and methane peaks at a FWHM of about 7.5 km. In each of these cases, a trade-off was made between the oscillatory nature of the retrieval and the resolution, with the current settings selected as the most appropriate compromise.

The reason for the larger-regularization requirement is unclear. It may be related to the retrieval setup using all windows for all altitudes, which is not the case for the MIPAS retrievals, where certain altitude–microwindow combinations were excluded because of radiometric interference from other species (von Clarmann et al., 2009). Not selecting

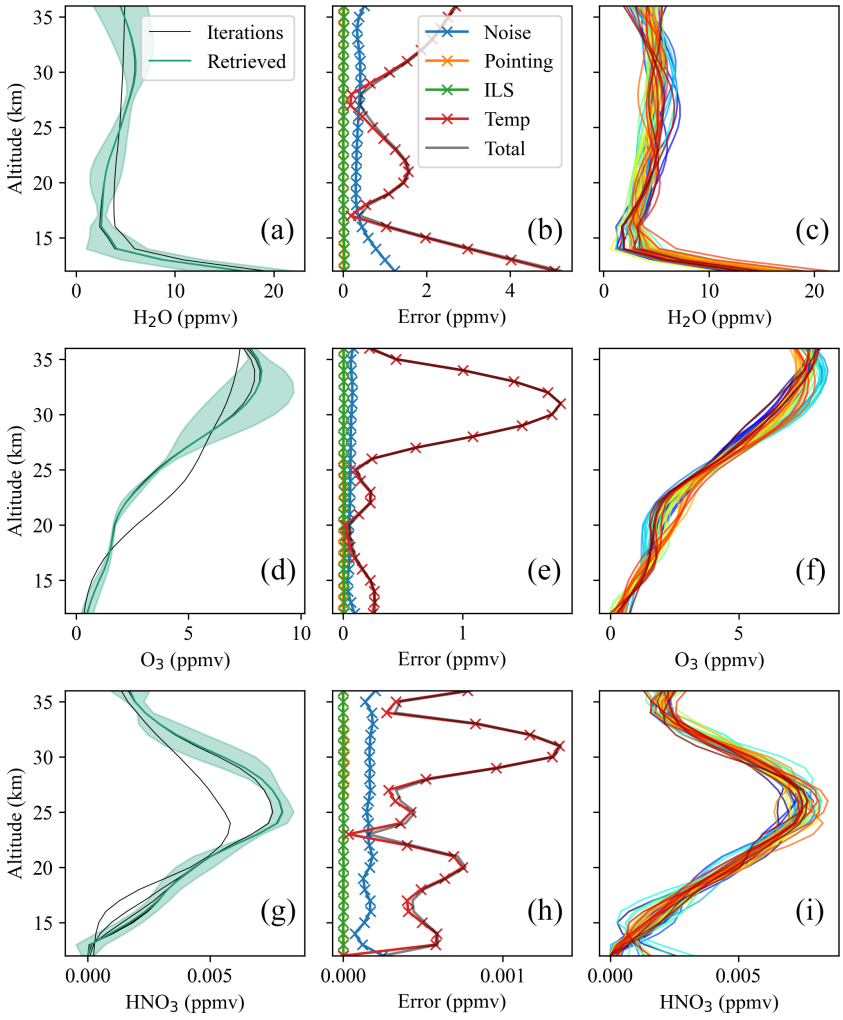

Figure 8. The results of the third stage for each of H_2O, O_3, and HNO_3 in green in the left-hand-side subfigures **(c, f, i)**, with each iteration shown in black and the associated errors in the center figures **(b, e, h)**. The shaded regions indicate the total error from all sources around a representative retrieved profile. The right-most panel **(a, d, g)** shows all retrievals over the time period 06:21:05 to 08:00:59 UTC on 1 September 2019.

for specific microwindow–altitude combinations may lead to a result where the LIFE retrievals are trying to fit too many measurements and optimize inefficiently. The use of particular microwindows for different altitudes is identified as an area of further exploration in the LIFE instrument and its descendants.

The remaining species, O_3, HNO_3, and N_2O, are shown to each have much smaller FWHM values and better vertical resolution with a value at or below 5 km for the entire range, with the exception of ozone, which peaks at around 6 km at upper altitudes.

5 Comparisons to ACE and MLS

Observations obtained with the ACE-FTS instrument several days after the LIFE demonstration flight and MLS observations on the flight day are plotted with the corresponding LIFE observations in Fig. 11. Nine ACE-FTS profiles that cover a time range from 6 to 9 September 2019, with a longitude range from −56 to −105° and a latitude range from 43 to 52°, are used in this comparison. Three MLS profiles from 1 September 2019, with a longitude range of −75 to −77° and a latitude range of 47 to 51°, are also used in the comparison. The Timmins flight took place from 31 August at 02:00 UTC until 1 September at 16:45 UTC in 2019, with the specific retrievals used in this paper being derived from measurements taking place between 06:21:05 and 08:00:59 UTC. The general location during flight was about 48° latitude and −81° longitude.

For the sake of comparison, the mean and standard deviation of the LIFE retrievals have been found and plotted alongside the ACE and MLS profiles. Figure 11 shows the side-

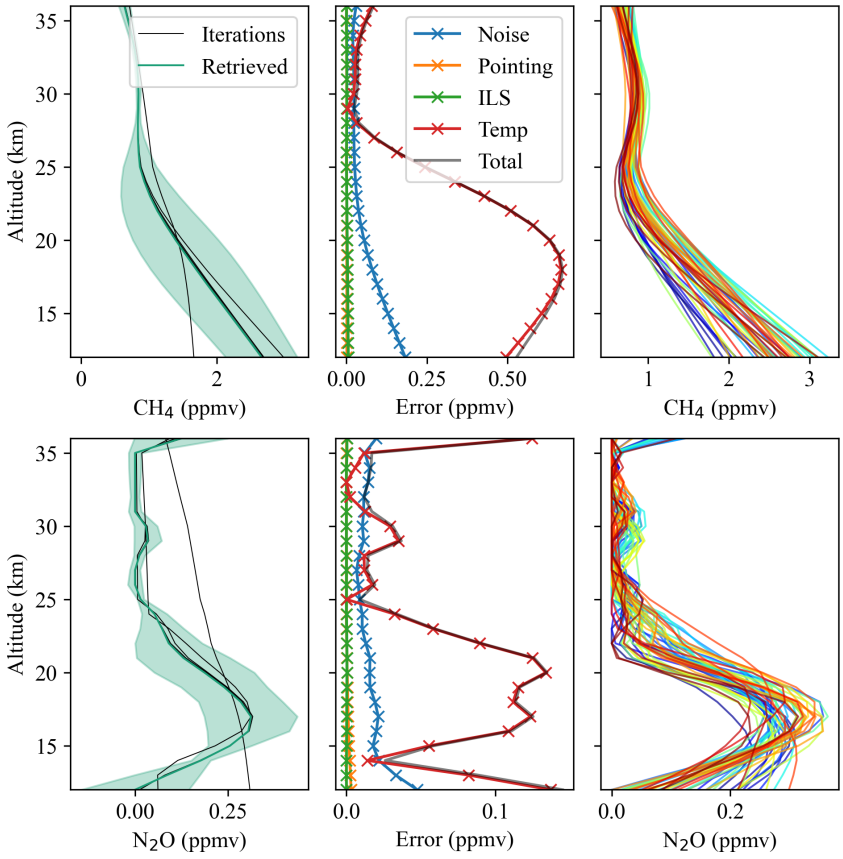

Figure 9. Third-stage trace-gas-vertical-profile results for CH_4 and N_2O, which were co-retrieved, along with their major error contributors. The shaded regions indicate the total error from all sources around a representative retrieved profile. The right-most panel shows all retrievals over the time period 06:21:05 to 08:00:59 UTC on 1 September 2019.

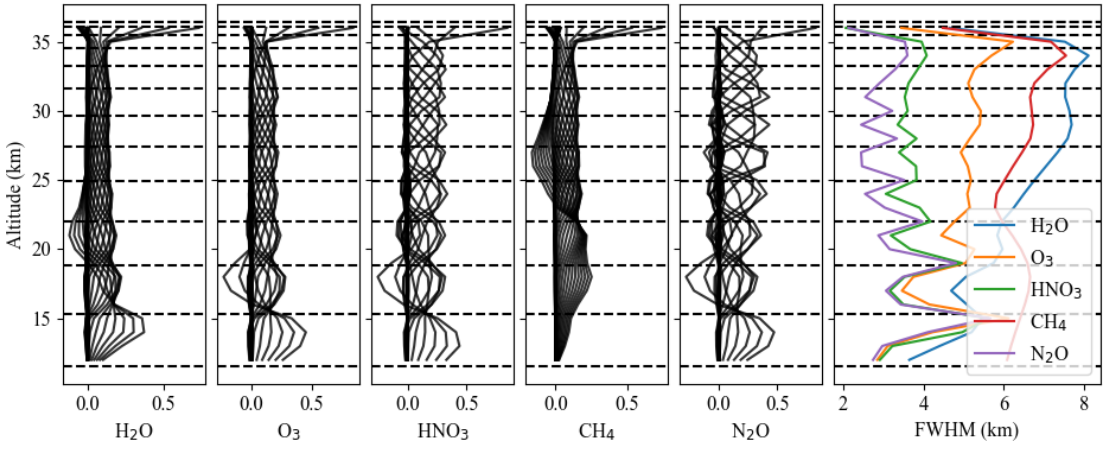

Figure 10. The averaging kernels for each of the LIFE retrieval species and the overplot of the vertical resolution for each, determined by the FWHM of the averaging kernels for each altitude grid point.

by-side comparison of the mean profile for a given species (dark-green line) with an error (shaded green area) defined by the standard deviation, the ACE counterparts given in dashed blue, and MLS measurements given in red. From left to right, the species are H_2O, O_3, HNO_3, CH_4, and N_2O.

In the case of H_2O and O_3, the mean retrieval appears to have a low bias, especially at the higher altitudes, with the standard deviation not quite overlapping with the comparison profiles, seeming to indicate a low bias in these atmospheric ranges. Ozone transitions to a high bias below 20 km

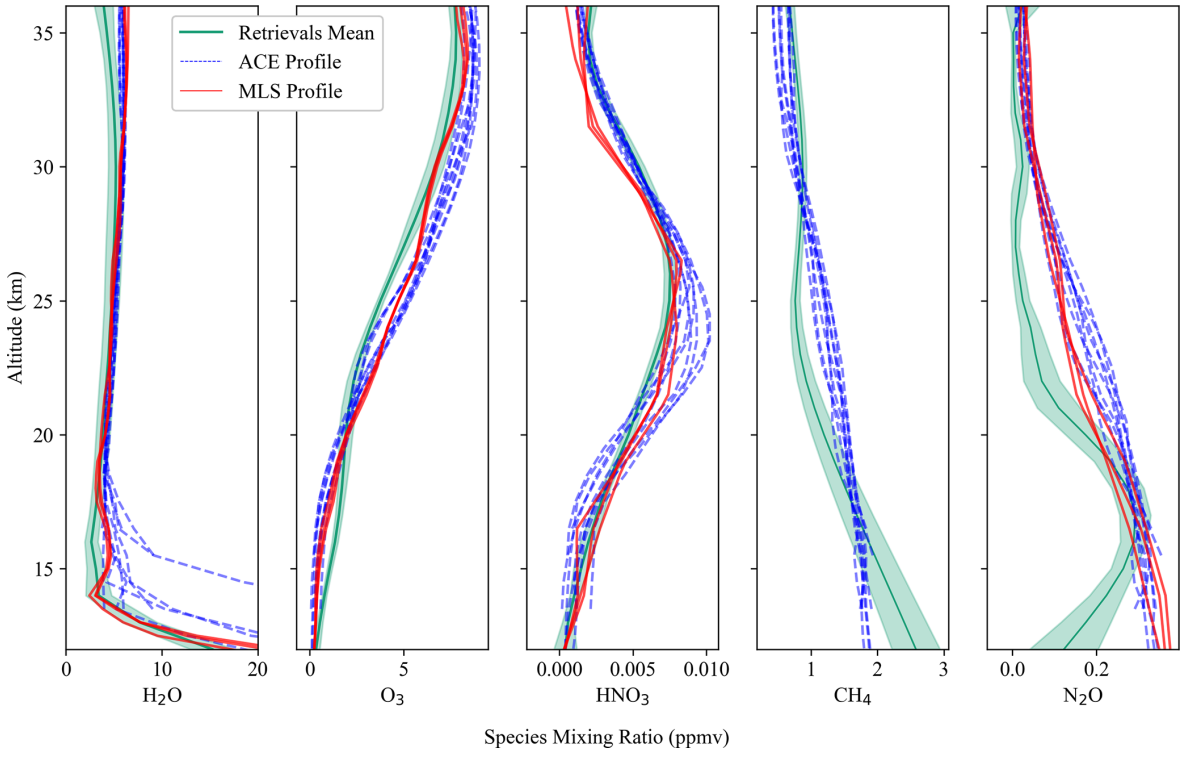

Figure 11. Comparison of each of the LIFE target trace gas average vertical profiles retrieved (green) on 1 September 2019 to the same species profiles as determined by the ACE instrument measurements (blue) in the time span of 6 to 9 September 2019 (longitude range −56 to −105° and latitude range 43 to 52°) and as determined by MLS observations (red) from 1 September 2019 (longitude range −75 to −77° and latitude range 47 to 51°; excluding CH_4).

altitude as well, which appears unique amongst the retrievals. The HNO_3 retrieval also appears to underestimate the peak at 25 km. The CH_4 and N_2O retrievals show the most deviation from the ACE measurements. For CH_4, there are some altitude regions for which the LIFE retrievals and ACE do not overlap, in the region where LIFE appears to have a low bias in the other species and in the region below the tropopause, which can be somewhat expected from the atmospheric variability in that region. N_2O shows less agreement, with a large bias towards lower values in the 20 to 30 km range before peaking at lower altitudes. It is likely that remaining systematic biases in the spectral region and the need for joint retrievals are exacerbating factors. The current version of the instrument clearly struggles with N_2O retrievals and with CH_4 to a lesser degree, but these results indicate that accurate profiles are a possibility if systematic biases can be removed. It should be noted that the closest ACE profile available was 6 September, 5 d after the Timmins flight, which could also account for some of the differences seen in all of the species. In general, the LIFE measurements show closer agreement with the MLS observations, though the same biases exist. A large part of this could be attributed to the temperature error in the profiles, as all species have high temperature dependence.

While there is not perfect agreement, the LIFE profiles for H_2O, O_3, and HNO_3 exhibit agreement in both shape and magnitude with the other instruments. The cause of the larger observed biases between the CH_4 and N_2O profiles remains unknown; residual errors in the radiometric correction in the microwindows are a possibility. The standard deviation exhibited across all retrievals is indicative of both instrument parameters and atmospheric variability over the course of the retrievals that are not fully understood and accounted for.

6 Conclusions

Instruments that make use of IFTS technology have been identified as promising candidates for furthering the understanding of the UTLS region of the atmosphere. The LIFE prototype instrument successfully demonstrates how the methodology can be implemented with commercially available off-the-shelf components with reduced complexity while still obtaining reliable trace gas retrievals. The successful flight in Timmins in August 2019 demonstrates that such an instrument is capable of being flown in the near-space environment. The atmospheric trace gas profiles obtained and their similarity to ACE and MLS measurements taken at a similar time and place indicate that the data taken from such

a platform also provide reliable scientific data. For these reasons, the pursuit of further instrumentation aboard a satellite platform and the creation of a LIFE successor are justifiable.

The major weakness identified with the trace gas retrievals is the need for further radiometric correction. Originally identified in the companion publication detailing the instrument characterization, artefacts that remain after the initial radiometric correction required additional steps to correct and are a likely source of error in the trace gas profiles obtained that are not encapsulated by the expected instrument error. The blackbodies used in the calibration during flight are identified as the cause of radiometric calibration error, as they were not originally purpose-built for the LIFE instrument. Another consideration is that a deep-space measurement is helpful in identifying and eliminating non-linear effects on the radiometric calibration, which the prototype was unable to take. Future iterations taking these factors into account with custom modifications will avoid the issues encountered with the LIFE prototype.

The scientific goal of the prototype LIFE instrument was to demonstrate that commercially available IFTS technology with reduced thermo-optic complexity produces valid atmospheric measurements that can be used for atmospheric-trace-gas-profile retrievals. The goal for validation identified H_2O, O_3, CH_4, and N_2O as the greenhouse gases most important to the understanding of the UTLS region while also being relatively straightforward for the instrument to measure. Based on the demonstration flight, HNO_3 was added due to its strong signal, and though not included in this publication, there is a potential for further retrievals of other atmospheric constituents. The presented results indicate that LIFE exceeded the initial goals, demonstrating the feasibility of a satellite-borne version of an instrument using the same methodology.

Code availability. The code used is available upon request.

Data availability. The dataset used in this analysis is available on Zenodo at https://doi.org/10.5281/zenodo.8061648 (Runge et al., 2023).

Author contributions. ER was responsible for formal analysis, investigation, software, and writing the original draft. JL was responsible for investigation. DZ was responsible for methodology. AB was responsible for methodology and conceptualization. DD was responsible for conceptualization. All listed authors were responsible for the review and editing process.

Competing interests. The contact author has declared that none of the authors has any competing interests.

Disclaimer. Publisher's note: Copernicus Publications remains neutral with regard to jurisdictional claims in published maps and institutional affiliations.

Acknowledgements. This study was made possible by collaboration with ABB Canada through the provision of components.

Financial support. This research has been supported by the Canadian Space Agency (CSA) Flights and Fieldwork for the Advancement of Space Technology (FAST; grant no. 15FASTA04) and Mathematics of Information Technology and Complex Systems (MITACS; grant no. FR25674).

Review statement. This paper was edited by Jian Xu and reviewed by two anonymous referees.

References

Anderson, G. P., Clough, S. A., Kneizys, F. X., Chetwynd, J. H., and Shettle, E. P.: AFGL (Air Force Geophysical Laboratory) atmospheric constituent profiles (0.120 km), Environmental research papers, Tech. rep., AFGL (Air Force Geophysical Laboratory), https://www.osti.gov/biblio/6862535 (last access: 14 January 2023), 1986.

Barnes, J. E., Kaplan, T., Vömel, H., and Read, W. G.: NASA/Aura/Microwave Limb Sounder water vapor validation at Mauna Loa Observatory by Raman lidar, J. Geophys. Res.-Atmos., 113, D15S03, https://doi.org/10.1029/2007JD008842, 2008.

Bernath, P. F., McElroy, C. T., Abrams, M. C., Boone, C. D., Butler, M., Camy-Peyret, C., Carleer, M., Clerbaux, C., Coheur, P.-F., Colin, R., DeCola, P., DeMazière, M., Drummond, J. R., Dufour, D., Evans, W. F. J., Fast, H., Fussen, D., Gilbert, K., Jennings, D. E., Llewellyn, E. J., Lowe, R. P., Mahieu, E., McConnell, J. C., McHugh, M., McLeod, S. D., Michaud, R., Midwinter, C., Nassar, R., Nichitiu, F., Nowlan, C., Rinsland, C. P., Rochon, Y. J., Rowlands, N., Semeniuk, K., Simon, P., Skelton, R., Sloan, J. J., Soucy, M.-A., Strong, K., Tremblay, P., Turnbull, D., Walker, K. A., Walkty, I., Wardle, D. A., Wehrle, V., Zander, R., and Zou, J.: Atmospheric Chemistry Experiment (ACE): Mission overview, Geophys. Res. Lett., 32, L15S01, https://doi.org/10.1029/2005GL022386, 2005.

Bognar, K., Zhao, X., Strong, K., Boone, C. D., Bourassa, A. E., Degenstein, D. A., Drummond, J. R., Duff, A., Goutail, F., Griffin, D., Jeffery, P. S., Lutsch, E., Manney, G. L., McElroy, C. T., McLinden, C. A., Millán, L. F., Pazmino, A., Sioris, C. E., Walker, K. A., and Zou, J.: Updated validation of ACE and OSIRIS ozone and NO_2 measurements in the Arctic using ground-based instruments at Eureka, Canada, J. Quant. Spectrosc. Ra., 238, 106571, https://doi.org/10.1016/j.jqsrt.2019.07.014, 2019.

Bourassa, A. E., Degenstein, D. A., and Llewellyn, E. J.: SASKTRAN: A spherical geometry radiative transfer code for efficient estimation of limb scattered sunlight, J. Quant. Spectrosc. Ra., 109, 52–73, https://doi.org/10.1016/j.jqsrt.2007.07.007, 2008.

Clough, S. A., Kneizys, F. X., Anderson, G. P., Shettle, E. P., and Chetwynd, J. H.: Software survey section, Software package JQSRT-O09-S87 FASCOD2 (Fast Atmospheric Signature CODE), J. Quant. Spectrosc. Ra., 37, I–IV, https://doi.org/10.1016/S0022-4073(87)90207-X, 1987.

Davis, S. M., Damadeo, R., Flittner, D., Rosenlof, K. H., Park, M., Randel, W. J., Hall, E. G., Huber, D., Hurst, D. F., Jordan, A. F., Kizer, S., Millan, L. F., Selkirk, H., Taha, G., Walker, K. A., and Vömel, H.: Validation of SAGE III/ISS Solar Water Vapor Data With Correlative Satellite and Balloon-Borne Measurements, J. Geophys. Res.-Atmos., 126, e2020JD033803, https://doi.org/10.1029/2020JD033803, 2021.

Fischer, H. and Oelhaf, H.: Remote sensing of vertical profiles of atmospheric trace constituents with MIPAS limb-emission spectrometers, Appl. Optics, 35, 2787–2796, https://doi.org/10.1364/AO.35.002787, 1996.

Fischer, H., Birk, M., Blom, C., Carli, B., Carlotti, M., von Clarmann, T., Delbouille, L., Dudhia, A., Ehhalt, D., Endemann, M., Flaud, J. M., Gessner, R., Kleinert, A., Koopman, R., Langen, J., López-Puertas, M., Mosner, P., Nett, H., Oelhaf, H., Perron, G., Remedios, J., Ridolfi, M., Stiller, G., and Zander, R.: MIPAS: an instrument for atmospheric and climate research, Atmos. Chem. Phys., 8, 2151–2188, https://doi.org/10.5194/acp-8-2151-2008, 2008.

Fletcher, R.: A modified Marquardt subroutine for nonlinear least squares fitting, Tech. rep., Atomic Energy Research Establishment (AERE), Harwell, Berkshire, https://www.osti.gov/biblio/4667484 (last access: 16 June 2023), 1971.

Friedl-Vallon, F., Maucher, G., Seefeldner, M., Trieschmann, O., Kleinert, A., Lengel, A., Keim, C., Oelhaf, H., and Fischer, H.: Design and characterization of the balloon-borne Michelson Interferometer for Passive Atmospheric Sounding (MIPAS-B2), Appl. Optics, 43, 3335–3355, https://doi.org/10.1364/AO.43.003335, 2004.

Friedl-Vallon, F., Gulde, T., Hase, F., Kleinert, A., Kulessa, T., Maucher, G., Neubert, T., Olschewski, F., Piesch, C., Preusse, P., Rongen, H., Sartorius, C., Schneider, H., Schönfeld, A., Tan, V., Bayer, N., Blank, J., Dapp, R., Ebersoldt, A., Fischer, H., Graf, F., Guggenmoser, T., Höpfner, M., Kaufmann, M., Kretschmer, E., Latzko, T., Nordmeyer, H., Oelhaf, H., Orphal, J., Riese, M., Schardt, G., Schillings, J., Sha, M. K., Suminska-Ebersoldt, O., and Ungermann, J.: Instrument concept of the imaging Fourier transform spectrometer GLORIA, Atmos. Meas. Tech., 7, 3565–3577, https://doi.org/10.5194/amt-7-3565-2014, 2014.

Froidevaux, L., Jiang, Y. B., Lambert, A., Livesey, N. J., Read, W. G., Waters, J. W., Browell, E. V., Hair, J. W., Avery, M. A., McGee, T. J., Twigg, L. W., Sumnicht, G. K., Jucks, K. W., Margitan, J. J., Sen, B., Stachnik, R. A., Toon, G. C., Bernath, P. F., Boone, C. D., Walker, K. A., Filipiak, M. J., Harwood, R. S., Fuller, R. A., Manney, G. L., Schwartz, M. J., Daffer, W. H., Drouin, B. J., Cofield, R. E., Cuddy, D. T., Jarnot, R. F., Knosp, B. W., Perun, V. S., Snyder, W. V., Stek, P. C., Thurstans, R. P., and Wagner, P. A.: Validation of Aura Microwave Limb Sounder stratospheric ozone measurements, J. Geophys. Res.-Atmos., 113, D15S20, https://doi.org/10.1029/2007JD008771, 2008.

Global Modeling and Assimilation Office (GMAO): instM_2d_int_Nx: MERRA-2 Monthly Mean Vertically Integrated Diagnostics, Goddard Space Flight Center Distributed Active Archive Center (GSFC DAAC), Greenbelt, MD, USA, https://doi.org/10.5067/KVTU1A8BWFSJ (last access: 10 September 2021), 2015.

Gordon, I. E., Rothman, L. S., Hill, C., Kochanov, R. V., Tan, Y., Bernath, P. F., Birk, M., Boudon, V., Campargue, A., Chance, K. V., Drouin, B. J., Flaud, J. M., Gamache, R. R., Hodges, J. T., Jacquemart, D., Perevalov, V. I., Perrin, A., Shine, K. P., Smith, M. A. H., Tennyson, J., Toon, G. C., Tran, H., Tyuterev, V. G., Barbe, A., Császár, A. G., Devi, V. M., Furtenbacher, T., Harrison, J. J., Hartmann, J. M., Jolly, A., Johnson, T. J., Karman, T., Kleiner, I., Kyuberis, A. A., Loos, J., Lyulin, O. M., Massie, S. T., Mikhailenko, S. N., Moazzen-Ahmadi, N., Müller, H. S. P., Naumenko, O. V., Nikitin, A. V., Polyansky, O. L., Rey, M., Rotger, M., Sharpe, S. W., Sung, K., Starikova, E., Tashkun, S. A., Auwera, J. V., Wagner, G., Wilzewski, J., Wcisło, P., Yu, S., and Zak, E. J.: The HITRAN2016 molecular spectroscopic database, J. Quant. Spectrosc. Ra., 203, 3–69, https://doi.org/10.1016/j.jqsrt.2017.06.038, 2017.

Hurst, D. F., Lambert, A., Read, W. G., Davis, S. M., Rosenlof, K. H., Hall, E. G., Jordan, A. F., and Oltmans, S. J.: Validation of Aura Microwave Limb Sounder stratospheric water vapor measurements by the NOAA frost point hygrometer, J. Geophys. Res.-Atmos., 119, 1612–1625, https://doi.org/10.1002/2013JD020757, 2014.

Jensen, K.: The Inclusion of Thermal Emissions Within the SASKTRAN Framework, PhD thesis, University of Saskatchewan, https://harvest.usask.ca/handle/10388/ETD-2015-03-1967 (last access: 26 October 2022), 2015.

Jiang, Y. B., Froidevaux, L., Lambert, A., Livesey, N. J., Read, W. G., Waters, J. W., Bojkov, B., Leblanc, T., McDermid, I. S., Godin-Beekmann, S., Filipiak, M. J., Harwood, R. S., Fuller, R. A., Daffer, W. H., Drouin, B. J., Cofield, R. E., Cuddy, D. T., Jarnot, R. F., Knosp, B. W., Perun, V. S., Schwartz, M. J., Snyder, W. V., Stek, P. C., Thurstans, R. P., Wagner, P. A., Allaart, M., Andersen, S. B., Bodeker, G., Calpini, B., Claude, H., Coetzee, G., Davies, J., De Backer, H., Dier, H., Fujiwara, M., Johnson, B., Kelder, H., Leme, N. P., König-Langlo, G., Kyro, E., Laneve, G., Fook, L. S., Merrill, J., Morris, G., Newchurch, M., Oltmans, S., Parrondos, M. C., Posny, F., Schmidlin, F., Skrivankova, P., Stubi, R., Tarasick, D., Thompson, A., Thouret, V., Viatte, P., Vömel, H., von Der Gathen, P., Yela, M., and Zablocki, G.: Validation of Aura Microwave Limb Sounder Ozone by ozonesonde and lidar measurements, J. Geophys. Res.-Atmos., 112, D24S34, https://doi.org/10.1029/2007JD008776, 2007.

Johansson, S., Woiwode, W., Höpfner, M., Friedl-Vallon, F., Kleinert, A., Kretschmer, E., Latzko, T., Orphal, J., Preusse, P., Ungermann, J., Santee, M. L., Jurkat-Witschas, T., Marsing, A., Voigt, C., Giez, A., Krämer, M., Rolf, C., Zahn, A., Engel, A., Sinnhuber, B.-M., and Oelhaf, H.: Airborne limb-imaging measurements of temperature, HNO_3, O_3, $ClONO_2$, H_2O and CFC-12 during the Arctic winter 2015/2016: characterization, in situ validation and comparison to Aura/MLS, Atmos. Meas. Tech., 11, 4737–4756, https://doi.org/10.5194/amt-11-4737-2018, 2018.

Kaufmann, M., Blank, J., Guggenmoser, T., Ungermann, J., Engel, A., Ern, M., Friedl-Vallon, F., Gerber, D., Grooß, J. U., Guenther, G., Höpfner, M., Kleinert, A., Kretschmer, E., Latzko, Th., Maucher, G., Neubert, T., Nordmeyer, H., Oelhaf, H., Olschewski, F., Orphal, J., Preusse, P., Schlager, H., Schneider, H., Schuettemeyer, D., Stroh, F., Suminska-Ebersoldt, O., Vogel,

B., M. Volk, C., Woiwode, W., and Riese, M.: Retrieval of three-dimensional small-scale structures in upper-tropospheric/lower-stratospheric composition as measured by GLORIA, Atmos. Meas. Tech., 8, 81–95, https://doi.org/10.5194/amt-8-81-2015, 2015.

Kleinert, A., Friedl-Vallon, F., Guggenmoser, T., Höpfner, M., Neubert, T., Ribalda, R., Sha, M. K., Ungermann, J., Blank, J., Ebersoldt, A., Kretschmer, E., Latzko, T., Oelhaf, H., Olschewski, F., and Preusse, P.: Level 0 to 1 processing of the imaging Fourier transform spectrometer GLORIA: generation of radiometrically and spectrally calibrated spectra, Atmos. Meas. Tech., 7, 4167–4184, https://doi.org/10.5194/amt-7-4167-2014, 2014.

Lambert, A., Read, W. G., Livesey, N. J., Santee, M. L., Manney, G. L., Froidevaux, L., Wu, D. L., Schwartz, M. J., Pumphrey, H. C., Jimenez, C., Nedoluha, G. E., Cofield, R. E., Cuddy, D. T., Daffer, W. H., Drouin, B. J., Fuller, R. A., Jarnot, R. F., Knosp, B. W., Pickett, H. M., Perun, V. S., Snyder, W. V., Stek, P. C., Thurstans, R. P., Wagner, P. A., Waters, J. W., Jucks, K. W., Toon, G. C., Stachnik, R. A., Bernath, P. F., Boone, C. D., Walker, K. A., Urban, J., Murtagh, D., Elkins, J. W., and Atlas, E.: Validation of the Aura Microwave Limb Sounder middle atmosphere water vapor and nitrous oxide measurements, J. Geophys. Res.-Atmos., 112, D24S36, https://doi.org/10.1029/2007JD008724, 2007.

Monte, C., Gutschwager, B., Adibekyan, A., Kehrt, M., Ebersoldt, A., Olschewski, F., and Hollandt, J.: Radiometric calibration of the in-flight blackbody calibration system of the GLORIA interferometer, Atmos. Meas. Tech., 7, 13–27, https://doi.org/10.5194/amt-7-13-2014, 2014.

Olschewski, F., Ebersoldt, A., Friedl-Vallon, F., Gutschwager, B., Hollandt, J., Kleinert, A., Monte, C., Piesch, C., Preusse, P., Rolf, C., Steffens, P., and Koppmann, R.: The in-flight blackbody calibration system for the GLORIA interferometer on board an airborne research platform, Atmos. Meas. Tech., 6, 3067–3082, https://doi.org/10.5194/amt-6-3067-2013, 2013.

Piesch, C., Sartorius, C., Friedl-Vallon, F., Gulde, T., Heger, S., Kretschmer, E., Maucher, G., Nordmeyer, H., Barthel, J., Ebersoldt, A., Graf, F., Hase, F., Kleinert, A., Neubert, T., and Schillings, H. J.: The mechanical and thermal setup of the GLORIA spectrometer, Atmos. Meas. Tech., 8, 1773–1787, https://doi.org/10.5194/amt-8-1773-2015, 2015.

Plieninger, J., Laeng, A., Lossow, S., von Clarmann, T., Stiller, G. P., Kellmann, S., Linden, A., Kiefer, M., Walker, K. A., Noël, S., Hervig, M. E., McHugh, M., Lambert, A., Urban, J., Elkins, J. W., and Murtagh, D.: Validation of revised methane and nitrous oxide profiles from MIPAS–ENVISAT, Atmos. Meas. Tech., 9, 765–779, https://doi.org/10.5194/amt-9-765-2016, 2016.

Riese, M., Oelhaf, H., Preusse, P., Blank, J., Ern, M., Friedl-Vallon, F., Fischer, H., Guggenmoser, T., Höpfner, M., Hoor, P., Kaufmann, M., Orphal, J., Plöger, F., Spang, R., Suminska-Ebersoldt, O., Ungermann, J., Vogel, B., and Woiwode, W.: Gimballed Limb Observer for Radiance Imaging of the Atmosphere (GLORIA) scientific objectives, Atmos. Meas. Tech., 7, 1915–1928, https://doi.org/10.5194/amt-7-1915-2014, 2014.

Rodgers, C. D.: Inverse Methods For Atmospheric Sounding: Theory And Practice, World Scientific, Oxford, https://doi.org/10.1142/3171, 2000.

Runge, E., Langille, J., Schentag, C., Bourassa, A., Letros, D., Loewen, P., Lloyd, N., Degenstein, D., and Grandmont, F.: A balloon-borne imaging Fourier transform spectrometer for atmospheric trace gas profiling, Rev. Sci. Instrum., 92, 094502, https://doi.org/10.1063/5.0060125, 2021.

Runge, E., Langille, J., Zawada, D., Bourassa, A., and Degenstein, D.: Spectral data used in "Stratospheric-trace-gas-profile retrievals from balloon-borne limb imaging of mid-infrared emission spectra", Zenodo [data set], https://doi.org/10.5281/zenodo.8061648, 2023.

Santee, M. L., Lambert, A., Read, W. G., Livesey, N. J., Cofield, R. E., Cuddy, D. T., Daffer, W. H., Drouin, B. J., Froidevaux, L., Fuller, R. A., Jarnot, R. F., Knosp, B. W., Manney, G. L., Perun, V. S., Snyder, W. V., Stek, P. C., Thurstans, R. P., Wagner, P. A., Waters, J. W., Muscari, G., de Zafra, R. L., Dibb, J. E., Fahey, D. W., Popp, P. J., Marcy, T. P., Jucks, K. W., Toon, G. C., Stachnik, R. A., Bernath, P. F., Boone, C. D., Walker, K. A., Urban, J., and Murtagh, D.: Validation of the Aura Microwave Limb Sounder HNO_3 measurements, J. Geophys. Res.-Atmos., 112, D24S40, https://doi.org/10.1029/2007JD008721, 2007.

Schwartz, M. J., Lambert, A., Manney, G. L., Read, W. G., Livesey, N. J., Froidevaux, L., Ao, C. O., Bernath, P. F., Boone, C. D., Cofield, R. E., Daffer, W. H., Drouin, B. J., Fetzer, E. J., Fuller, R. A., Jarnot, R. F., Jiang, J. H., Jiang, Y. B., Knosp, B. W., Krüger, K., Li, J.-L. F., Mlynczak, M. G., Pawson, S., Russell III, J. M., Santee, M. L., Snyder, W. V., Stek, P. C., Thurstans, R. P., Tompkins, A. M., Wagner, P. A., Walker, K. A., Waters, J. W., and Wu, D. L.: Validation of the Aura Microwave Limb Sounder temperature and geopotential height measurements, J. Geophys. Res.-Atmos., 113, D15S11, https://doi.org/10.1029/2007JD008783, 2008.

Sha, M. K.: Characterization and Optimization of the new Imaging Fourier Transform Spectrometer GLORIA, PhD thesis, Karlsruhe Institute of Technology, https://doi.org/10.5445/IR/1000038372, 2013.

Sheese, P. E., Walker, K. A., Boone, C. D., Bernath, P. F., Froidevaux, L., Funke, B., Raspollini, P., and von Clarmann, T.: ACE-FTS ozone, water vapour, nitrous oxide, nitric acid, and carbon monoxide profile comparisons with MIPAS and MLS, J. Quant. Spectrosc. Ra., 186, 63–80, https://doi.org/10.1016/j.jqsrt.2016.06.026, 2017.

Sheese, P. E., Walker, K. A., Boone, C. D., Bourassa, A. E., Degenstein, D. A., Froidevaux, L., McElroy, C. T., Murtagh, D., Russell III, J. M., and Zou, J.: Assessment of the quality of ACE-FTS stratospheric ozone data, Atmos. Meas. Tech., 15, 1233–1249, https://doi.org/10.5194/amt-15-1233-2022, 2022.

Ungermann, J., Blank, J., Dick, M., Ebersoldt, A., Friedl-Vallon, F., Giez, A., Guggenmoser, T., Höpfner, M., Jurkat, T., Kaufmann, M., Kaufmann, S., Kleinert, A., Krämer, M., Latzko, T., Oelhaf, H., Olchewski, F., Preusse, P., Rolf, C., Schillings, J., Suminska-Ebersoldt, O., Tan, V., Thomas, N., Voigt, C., Zahn, A., Zöger, M., and Riese, M.: Level 2 processing for the imaging Fourier transform spectrometer GLORIA: derivation and validation of temperature and trace gas volume mixing ratios from calibrated dynamics mode spectra, Atmos. Meas. Tech., 8, 2473–2489, https://doi.org/10.5194/amt-8-2473-2015, 2015.

von Clarmann, T., Höpfner, M., Kellmann, S., Linden, A., Chauhan, S., Funke, B., Grabowski, U., Glatthor, N., Kiefer, M., Schieferdecker, T., Stiller, G. P., and Versick, S.: Retrieval of temperature, H_2O, O_3, HNO_3, CH_4, N_2O, $ClONO_2$ and ClO from MIPAS reduced resolution nominal mode limb emission measurements,

Atmos. Meas. Tech., 2, 159–175, https://doi.org/10.5194/amt-2-159-2009, 2009.

Vömel, H., Barnes, J. E., Forno, R. N., Fujiwara, M., Hasebe, F., Iwasaki, S., Kivi, R., Komala, N., Kyrö, E., Leblanc, T., Morel, B., Ogino, S.-Y., Read, W. G., Ryan, S. C., Saraspriya, S., Selkirk, H., Shiotani, M., Valverde Canossa, J., and Whiteman, D. N.: Validation of Aura Microwave Limb Sounder water vapor by balloon-borne Cryogenic Frost point Hygrometer measurements, J. Geophys. Res.-Atmos., 112, D24S37, https://doi.org/10.1029/2007JD008698, 2007.

Walker, K. A., Randall, C. E., Trepte, C. R., Boone, C. D., and Bernath, P. F.: Initial validation comparisons for the Atmospheric Chemistry Experiment (ACE-FTS), Geophys. Res. Lett., 32, L16S04, https://doi.org/10.1029/2005GL022388, 2005.

Walker, K. A., Sheese, P. E., Zou, J., and Boone, C. D.: Long-term Validation for the Atmospheric Chemistry Experiment Fourier Transform Spectrometer (ACE-FTS), in: Light, Energy and the Environment 2018 (E2, FTS, HISE, SOLAR, SSL) (2018), paper FW5A.2, Optica Publishing Group, https://doi.org/10.1364/FTS.2018.FW5A.2, 2018.

Walker, K. A., Sheese, P. E., and Zou, J.: Validation Studies for the Atmospheric Chemistry Experiment Fourier Transform Spectrometer (ACE-FTS), in: OSA Optical Sensors and Sensing Congress 2021 (AIS, FTS, HISE, SENSORS, ES) (2021), paper FTh4G.4, Optica Publishing Group, https://doi.org/10.1364/FTS.2021.FTh4G.4, 2021.

Warnock, T.: The SASKTRAN Thermal Infrared Radiative Transfer Model with Analytic Jacobian Calculations, thesis, University of Saskatchewan, https://harvest.usask.ca/handle/10388/12963 (last access: 26 October 2022), 2020.

Waters, J., Froidevaux, L., Harwood, R., Jarnot, R., Pickett, H., Read, W., Siegel, P., Cofield, R., Filipiak, M., Flower, D., Holden, J., Lau, G., Livesey, N., Manney, G., Pumphrey, H., Santee, M., Wu, D., Cuddy, D., Lay, R., Loo, M., Perun, V., Schwartz, M., Stek, P., Thurstans, R., Boyles, M., Chandra, K., Chavez, M., Chen, G.-S., Chudasama, B., Dodge, R., Fuller, R., Girard, M., Jiang, J., Jiang, Y., Knosp, B., LaBelle, R., Lam, J., Lee, K., Miller, D., Oswald, J., Patel, N., Pukala, D., Quintero, O., Scaff, D., Van Snyder, W., Tope, M., Wagner, P., and Walch, M.: The Earth observing system microwave limb sounder (EOS MLS) on the aura Satellite, IEEE T. Geosci. Remote, 44, 1075–1092, https://doi.org/10.1109/TGRS.2006.873771, 2006.

Waymark, C., Walker, K., Boone, C. D., and Bernath, P. F.: ACE-FTS version 3.0 data set: validation and data processing update, Ann. Geophys., 56, 10, https://doi.org/10.4401/ag-6339, 2014.

Weaver, D., Strong, K., Walker, K. A., Sioris, C., Schneider, M., McElroy, C. T., Vömel, H., Sommer, M., Weigel, K., Rozanov, A., Burrows, J. P., Read, W. G., Fishbein, E., and Stiller, G.: Comparison of ground-based and satellite measurements of water vapour vertical profiles over Ellesmere Island, Nunavut, Atmos. Meas. Tech., 12, 4039–4063, https://doi.org/10.5194/amt-12-4039-2019, 2019.

Zawada, D. J., Dueck, S. R., Rieger, L. A., Bourassa, A. E., Lloyd, N. D., and Degenstein, D. A.: High-resolution and Monte Carlo additions to the SASKTRAN radiative transfer model, Atmos. Meas. Tech., 8, 2609–2623, https://doi.org/10.5194/amt-8-2609-2015, 2015.

Zawada, D. J., Bourassa, A. E., and Degenstein, D. A.: Two-dimensional analytic weighting functions for limb scattering, J. Quant. Spectrosc. Ra., 200, 125–136, https://doi.org/10.1016/j.jqsrt.2017.06.008, 2017.